

Hierarchically structured functional porous silica and composite produced by evaporation-induced self-assembly

Hongyou Fan ^{a,b}, Scott Reed ^b, Tom Baer ^b, Randy Schunk ^b, Gabriel P. López ^a,
C. Jeffrey Brinker ^{a,b,*}

^a *Department of Chemical and Nuclear Engineering, Center for Micro-Engineered Materials, The University of New Mexico, Albuquerque, NM 87131, USA*

^b *Sandia National Laboratories, Albuquerque, NM 87185, USA*

Received 11 May 2000; accepted 5 June 2000

Abstract

Recently so-called soft lithography approaches [Angew. Chem. Int. Ed. 37 (1998) 550] have been combined with surfactant [Adv. Mater. 9 (1997) 811, Nature 390 (1997) 674] and particulate [Science 282 (1998) 2244] templating procedures to create oxides with multiple levels of structural order. But the materials thus formed have been limited primarily to oxides with no specific functionality, and the associated processing times have ranged from hours to days. Using self-assembling inks we have combined evaporation-induced (silica/surfactant) self-assembly [Adv. Mater. 11 (1999) 579] with rapid prototyping techniques like micro-pen lithography [Science 283 (1999) 661, Mat. Res. Soc. Symp. Proc. 542 (1999) 159], ink-jet printing [Adv. Mater. 11 (1999) 734, Mat. Sci. Eng. C5 (1998) 289], and dip coating on micro-contact printed substrates to form hierarchically organized structures in seconds. By co-condensation of tetra-functional silanes (Si(OR)₄) with tri-functional organosilanes ((RO)₃SiR') [Chem. Commun. (1999) 1367, Chem. Commun. (1997) 1769, J. Am. Chem. Soc. 119 (1997) 4090] or bridged silsesquioxanes (RO)₃Si–R'–Si(OR)₃ or by inclusion of organic additives, we have selectively derivatized the silica framework with functional R' ligands or molecules. The rapid-prototyping procedures we describe are simple, employ readily available equipment, and provide a link between computer-aided design and self-assembled functional nanostructures. We expect that the ability to form arbitrary functional designs on arbitrary surfaces will be of practical importance for directly writing sensor arrays and fluidic or photonic systems. © 2001 Elsevier Science B.V. All rights reserved.

Keywords: Surfactant self-assembly; Mesoporous; Micro-pen writing; Ink-jet printing; Selective de-wetting

1. Introduction

Living systems exhibit form and function on multiple length scales and at multiple locations. In order to mimic such natural designs and impart life-like qualities to man-made materials, it is necessary to develop efficient strategies for assembling hierarchical materials. Conventional photolithography, although ubiquitous in the

* Corresponding author. Address: Department of Chemistry and Nuclear Engineering, Center for Micro-Engineered Materials, The University of New Mexico, Albuquerque, NM 87131, USA.

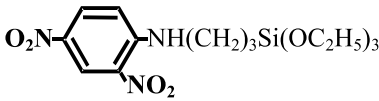
fabrication of microelectronics and MEMS, is impractical for defining features sizes below 0.1 μm and poorly suited to pattern chemical functionality. Since the discovery of surfactant-templated silica mesophases [13], considerable effort has been devoted to the development of molecular scale, organic modification schemes to impart useful functionality to the pore surfaces [10,12,14–19]. Concurrently a variety of patterning strategies have been developed to define macroscopically the shapes of deposited thin-film mesophases and their locations on the substrate surface [2–4]. Our approach combines molecular scale, evaporation-induced self-assembly (EISA) [5] of organically-modified mesophases [10,12,14–19] with macroscopic, evaporative, printing procedures. We report the rapid fabrication of hierarchical structures exhibiting form and function on multiple length scales and at multiple locations. At the molecular scale, functional organic moieties (Table 1) are positioned on pore surfaces; on the meso-scale, mono-sized pores are organized into one-, two-, or three-dimensional networks, providing

size-selective accessibility from the gas or liquid phase; and on the macroscale, two-dimensional (2D) arrays and fluidic or photonic systems are defined.

2. Experimental

Precursor solutions used as inks were prepared by addition of surfactants (cationic, CTAB; $\text{CH}_3(\text{CH}_2)_{15}\text{N}^+(\text{CH}_3)_3\text{Br}^-$ or non-ionic, Brij-56; $\text{CH}_3(\text{CH}_2)_{15}-(\text{OCH}_2\text{CH}_2)_{10}-\text{OH}$ and Pluronic P123, $\text{HO}(\text{CH}_2\text{CH}_2\text{O})_{20}(\text{CH}(\text{CH}_3)\text{CH}_2\text{O})_{70}-(\text{CH}_2\text{CH}_2\text{O})_{20}-\text{H}$), organosilanes ($\text{R}'-\text{Si}(\text{OR})_3$, see Table 1), or organic molecules (see Table 1) to an acidic silica sol prepared from TEOS [$\text{Si}(\text{OCH}_2\text{CH}_3)_4$] (A2^{**}). The acid concentration employed in the A2^{**} synthesis procedure was chosen to minimize the siloxane condensation rate, thereby promoting facile self-assembly during printing [20]. In a typical preparation, TEOS, ethanol, water and dilute HCl (mole ratios: 1:3.8:1:5 $\times 10^{-5}$) were refluxed at 60°C for 90 min.

Table 1
Functional organosilanes and properties of resultant thin film mesophases

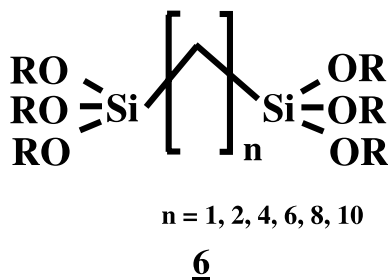
	Functional silanes ^a /additives ^b $\text{R}'-\text{Si}(\text{OR})_3$	Mesophase	Pore size ^c (\AA)	Surface area ^c (m^2/g)	Properties and applications
<u>1</u>	$\text{F}_3\text{C}(\text{CF}_2)_5\text{CH}_2\text{CH}_2\text{Si}(\text{OC}_2\text{H}_5)_3$ Tridecafluoro-1,1,2,2-tetrahydrooctyltriethoxysilane (TFTS)	3-dH	25	850	Hydrophobic; low k dielectrics
<u>2</u>	$\text{HS}-(\text{CH}_2)_3\text{Si}(\text{OCH}_3)_3$ Mercaptopropyltrimethoxysilane (MPS)	3-dH	25	1060	Coupling of noble metals
<u>3</u>	$\text{NH}_2-(\text{CH}_2)_3\text{Si}(\text{OCH}_3)_3$ Aminopropyltrimethoxysilane (APS)	Cubic	22	750	Coupling of noble metals, dye, and bioactive molecules
<u>4</u>	Dye^d – $\text{NH}-(\text{CH}_2)_3\text{Si}(\text{OCH}_3)_3$	Cubic	21	545	pH sensitive
<u>5</u>		3-dH	22	560	Chromophore; nonlinear optical material (χ^2)
<u>6</u>	$(\text{H}_5\text{C}_2\text{O})_3\text{SiCH}_2\text{CH}_2\text{Si}(\text{OC}_2\text{H}_5)_3$	Cubic	40	430	low k dielectrics

^a Functional groups are retained through selective surfactant removal during heat treatment in nitrogen. TGA and DTA were used to establish the appropriate temperature window enabling complete surfactant removal without silane decomposition.

^b Additives investigated include rhodamine-B, cytochrome c (from Fluka), oil blue N, disperse yellow 3 (from Aldrich), silver ions and silver nanoparticles.

^c Pore size and surface area were determined from N_2 sorption isotherms obtained at -196°C , using a SAW technique. Mass change due to nitrogen sorption was monitored ($\sim 80 \text{ pg cm}^{-2}$ sensitivity) as a function of nitrogen relative pressure. Pore size and surface area were determined from the isotherms using the BET equation and the BJH algorithm, respectively.

^d **4** was prepared by a conjugation reaction between a thin film mesophase containing **3** and the dye molecule (5,6-carboxyfluorecein, succinimidyl ester (5,6-FAM, SE) from Molecular Probes).



Scheme 1. Chemical formulae of bridged silsesquioxane monomers.

The sol was diluted with 2 volumes of ethanol followed by further addition of water and HCl. Organosilanes ($R'-Si(OR)_3$, where R' is a non-hydrolyzable organic functional ligand) were added followed by surfactants and (optionally) organic additives (see Table 1). Surfactants were added in requisite amounts to achieve initial surfactant concentrations c_0 ranging from 0.004 to 0.23 M ($c_0 \ll \text{cmc}$). The final reactant molar ratios were: 1 TEOS:22 C_2H_5OH :5 H_2O :0.093–0.31 surfactant:0.039–0.8 organosilanes: 2.6×10^{-5} organic additives. For the bridged silsesquioxane, $(RO)_3Si-R'-Si(OR)_3$ (molecules with different R' are shown in Scheme 1), the neat precursor was diluted in ethanol and mixed with 1–8 wt.% CTAB or Brij-56 surfactant followed by addition of an aqueous solution of HCl. The final reactant molar ratios were: Si:EtOH: H_2O :HCl:surfactant = 1:22:5:0.004:0.054–0.18. Co-hydrolysis of organosilanes with TEOS in the initial A2** sol preparation generally resulted in disordered worm-like mesostructures [21]. After pattern deposition and drying, the surfactant templates were selectively removed by calcination in a nitrogen atmosphere at a temperature sufficient to decompose the surfactant molecules ($\sim 350^\circ\text{C}$) without degrading the covalently bound organic ligands R' (confirmed by ^{29}Si Magic-angle Spinning (MAS) NMR spectroscopy) or by solvent extraction.

2.1. Patterning procedures

1. Micro-pen lithography (MPL) was performed using a Model 400a micropen instrument (Ohmcraft Inc., Pittsford, NY). The pen orifice was 50 μm and the writing speed was 2.54 cm/s.

The pattern was designed using AutoCAD software (AutoCAD release 14.01, Autodesk Inc., San Rafael, CA).

2. Ink-jet printing (IJP) was performed using a Model HP DeskJet 1200C printer (Hewlett-Packard Co., San Diego, CA). The pattern was designed using Microsoft PowerPoint 98 software.

3. Dip-coating of patterned (hydrophilic/hydrophobic) substrates was performed at a withdrawal speed of 7.6–51 cm min^{-1} under ambient laboratory conditions. Hydrophilic/hydrophobic patterns were created by micro-contact printing ($\mu\text{-CP}$) of hydrophobic, *n*-octadecyltrichlorosilane ($\text{CH}_3(\text{CH}_2)_{17}\text{SiCl}_3$) self assembled monolayers (SAMs) [22] on hydrophilic silicon substrates (hydroxylated native oxide) or by a technique involving electrochemical desorption of a hydroxyl-terminated SAM prepared from 11-mercaptoundecanol ($\text{HO}(\text{CH}_2)_{11}\text{SH}$) from patterned, electrically isolated gold electrodes followed by immersion in a 1 mM ethanolic solution of 1-dodecanethiol, $\text{CH}_3(\text{CH}_2)_{11}\text{SH}$ (Ref. [29]).

2.2. $\mu\text{-CP}$ of patterned surfaces

Polydimethylsiloxane (PDMS) stamps that have relief structures consisting of circles, triangles, and stripes were fabricated according to published procedures [1]. The stamp was first inked with a 1 mM solution of $\text{HS}(\text{CH}_2)_{11}\text{CH}_3$ in ethanol and dried in a nitrogen stream. The stamp was then put in contact with the surface of the gold substrate for 30 s. Fig. 1 illustrates the process of making the stamp and forming a patterned self-assembled monolayer on a gold surface, or silica surface, by $\mu\text{-CP}$. The hydrophobic thiol-derivatized sample was then washed with a 10 mM solution of $\text{HS}(\text{CH}_2)_{11}\text{OH}$ in ethanol to passivate the remaining area that had not contacted the stamp. Subsequently, the sample was rinsed with ethanol several times, then dried under a flow of nitrogen. For pattern fabrication on silicon wafers, a hydrophobic organosilane such as octadecyltrichlorosilane was used in hexane or toluene at a concentration of 10 mM. After first printing the

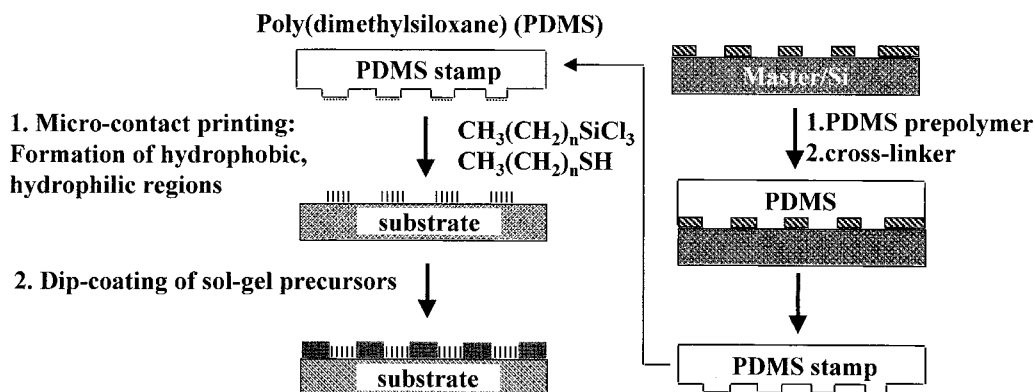


Fig. 1. Scheme of making of PDMS stamp and fabrication of patterns on gold and silica surfaces. (1) Micro-contact printing: formation of hydrophobic and hydrophilic regions. (2) dip coating of sol-gel precursors including silica, surfactant, water, and alcohol.

hydrophobic silane the wafer was washed with hexane several times, dried in a nitrogen stream, and then placed in an 80°C oven to cure and promote siloxane condensation. In this case, the amorphous, hydroxylated silica surface itself serves as a hydrophilic pattern (H_2O contact angle less than 10°).

2.3. Patterned surfaces by an electrochemical method

A wettable SAM was formed by immersing a 560 Å gold film in 1 mM ethanolic solution of 11-mercaptoundecanol (HOC11SH). After 1 min the SAM was dried under flowing nitrogen. Then a pulsed nitrogen-pumped dye laser emitting at 390 nm with a maximum intensity of 20 μJ/pulse (Laser Scissors from Cell Robotics, Albuquerque, NM) was focused on the gold surface through a microscope objective lens (Nikon Diaphot 300) to ablate the gold film and create interdigitized regions electrically isolated from one another. A reducing potential of -2.4 V versus silver wire reference in 0.5 M ethanolic potassium hydroxide was applied to desorb the 11-mercaptoundecanol (HOC11SH) from those regions in electrical contact with the electrodes. This left SAMs on regions electrically isolated from the reducing potential intact. Subsequent immersion of the sample in a 1 mM ethanolic solution of hexadecanethiol (C16SH) created a sample with wettable (hydro-

philic-OH terminated) and non-wettable (hydrophobic- CH_3 terminated) regions.

3. Results and discussion

Vital to rapid patterning procedures is the use of stable, homogeneous inks that on evaporation undergo self-assembly to form the desired organically modified silica-surfactant mesophase. For this purpose we prepared oligomeric silica sols in ethanol/water solvents at a hydronium ion concentration ($[\text{H}_3\text{O}^+] \approx 0.01$ M) designed to minimize the siloxane condensation rate, thereby enabling facile silica-surfactant self-assembly during the brief time span of the writing operation (several seconds). Surfactants were added at an initial concentration c_0 , much less than the critical micelle concentration, cmc, insuring homogeneity and longevity of the ink.

As a pattern of ink is metered onto a surface, preferential evaporation of ethanol causes enrichment of water, surfactant, and silicates, establishing a complex three-dimensional (3D; longitudinal and radial) gradient in their respective concentrations (see, e.g., the 3D finite-element simulation of pen lithography in Fig. 2b). Where the cmc is exceeded, cooperative silica-surfactant self-assembly creates micelles. Further evaporation, predominantly of water, promotes the continuous self-organization of micelles into silica-surfactant

liquid-crystalline mesophases. Incipient liquid-crystalline domains are nucleated at liquid–vapor interfaces [23] (at concentration $c < \text{cmc}$) and grow inward along compositional trajectories established by the steep, 3D evaporation-induced concentration gradient (Fig. 2).

The amphiphilic nature of some organosilanes like tridecafluoro-1,1,2,2-tetrahydrooctyltriethoxysilane (TFTS; compound **1** in Table 1) causes them to behave as co-surfactants, positioning the hydrophilic $\text{Si}(\text{OR})_x(\text{OH})_{3-x}$ headgroups in close proximity to the silica oligomers where they are incorporated into the framework upon further hydrolysis and condensation, thereby localizing covalently attached R' moieties on the pore surfaces. Using the general class of compounds referred to as bridged silsesquioxanes $(\text{RO})_3\text{Si}-\text{R}'-\text{Si}(\text{OR})_3$ (Scheme 1), we report the formation of a new class of polysilsesquioxane mesophases with integral organic functionality. In contrast to hybrid mesophases where organic ligands or molecules are situated on pore surfaces [10–12,14], this class of materials necessarily incorporates the organic constituents into the framework as molecularly dispersed bridging ligands. This new mesostructural organization is anticipated to result in synergistic properties derived from the molecular scale mixing of the inorganic and organic components. For example, the introduction of integral organic groups should impart toughness, hydrophobicity, and a reduced dielectric constant to the framework, while at the same time enhancing the thermal stability of the organic constituents. Such considerations are exceedingly important for current applications of silica mesophases like low dielectric constant (low k) coatings for the next generation of microelectronics, environmental sensors, and high temperature membranes. In order to establish structure-porosity

relationships, we prepared a series of films from TEOS and **6** ($n = 2$) with molar ratios TEOS:**6** = 75:25 (TB_1), 50:50 (TB_2), and 25:75 (TB_3). Synthesis and processing procedures were chosen to create isotropic disordered (worm-like) thin film mesophases [18] with comparable film thicknesses (measured by spectroscopic ellipsometry) and porosities (measured by analyses of SAW-based N_2 sorption isotherms). After calcination at 350°C under N_2 to remove the surfactant templates, all films were vapor treated with hexamethyldisilazane to avoid water adsorption. Table 2 compares values of the dielectric constants (measured using a standard capacitance–voltage technique employing a mercury probe), Young's modulus and hardness (modulus and hardness calculated from nanoindentation measurements at a constant indentation depth, assuming a Poisson's ratio of 0.2). We observe a consistent trend of increasing modulus and hardness and decreasing dielectric constant with substitution of the bridged silsesquioxane ($\equiv\text{Si}-(\text{CH}_2)_2-\text{Si}\equiv$) for siloxane ($\equiv\text{Si}-\text{O}-\text{Si}\equiv$) in the framework. This preliminary evidence suggests that introduction of integral organic groups into the frameworks of mesoporous materials can result in synergistic properties, promising an unprecedented ability to tune properties and function. The trend of increasing mechanical performance and decreasing dielectric constant observed here is of immediate and crucial interest to the burgeoning field of low k dielectrics.

Hydrophobic but alcohol-soluble organic molecules like rhodamine-B partition into the hydrophobic micellar interiors upon ethanol evaporation [24], and ultimately become compartmentalized within the channel network of the resulting mesophase. Retention of the covalently attached functional organic moieties after surfactant removal by pyrolysis was confirmed using

Table 2
Properties of calcined TEOS/ $(\equiv\text{Si}-(\text{CH}_2)_2-\text{Si}\equiv)$ mesoporous thin films prepared with 4 wt.% Brij-56 surfactant

Framework (TEOS:silsesquioxane)	Thickness (Å)	Dielectric constant	Porosity	Modulus (GPa)	Hardness (GPa)
TB_1 (75:25)	3135	2.15	56%	3.5	0.35
TB_2 (50:50)	3154	2.13	53%	3.7	0.39
TB_3 (25:75)	3015	1.98	56%	4.3	0.48

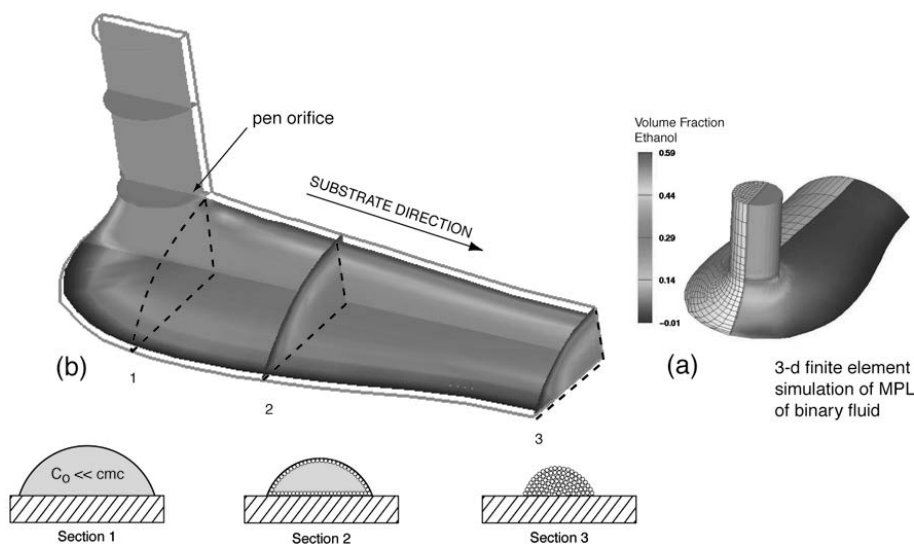


Fig. 2. MPL of a surfactant-templated mesophase. (a) Simulation of 3D, binary fluid pattern dispensed on a flat substrate with the following parameters: pen orifice, 50.0 μm ; substrate speed, 2.5 cm s^{-1} ; and fluid injection rate (inlet velocity), 4.0 cm s^{-1} . Color contours represent evaporation induced, 3D gradients in alcohol composition. Residence times for fluid elements entering at the pen orifice and exiting at Section 3 ranged from 0.23 to 0.30 ms. Fluid was modeled as 54 vol.% ethanol and 46 vol.% non-volatile phase with Reynolds number $Re = 1.25$ and $Ca = 0.000833$. An ad hoc value of 45° was chosen for the static contact angle. Note that this angle persists at all points on the dynamic contact line because of the dominance of surface tension at this low value of Ca . (b) The initially homogeneous sol metered on to the moving substrate experiences preferential evaporation of alcohol creating a complex 3D (longitudinal and radial) gradient in the concentrations of water and non-volatile surfactant and silicate species. Progressive enrichment of silica and surfactant induces micelle formation and subsequent growth of silica-surfactant mesophases inward from the liquid-vapor interface as recently demonstrated for aerosols [27]. The numerical method utilized for (a) and (b) consisted of a 3D finite-element discretization of the Navier–Stokes equations augmented with a 3D boundary-fitted mesh motion algorithm to track the free surface [31,32]. Special relations at the 3D dynamic wetting line were also applied.

^{29}Si MAS NMR spectroscopy. Fluorescence–imaging and ultraviolet–visible spectroscopy were used to confirm retention and functionality of optically active ligands and molecules.

Fig. 2 schematically illustrates direct writing of a mesoscopically ordered nanostructure, using MPL [7]. Fig. 3a shows a macroscopic pattern formed in several seconds by MPL of a rhodamine-B containing solution on a hydrophilic surface. The inset in Fig. 3a shows the corresponding fluorescence image of several adjacent stripes acquired through a 610 nm band pass filter, demonstrating retention of rhodamine-B functionality, and the transmission electron microscopy (TEM) image (Fig. 3b) reveals the ordered pore structure characteristic of a cubic thin-film mesophase. The MPL line width can vary from micrometers to millimeters. It depends on such

factors as pen dimension [6], wetting characteristics, evaporation rate, capillary number ($Ca = \text{ink viscosity} \times \text{substrate speed/surface tension}$) and ratio of the rates of ink supply and withdrawal (inlet velocity/substrate velocity). The effect of wetting has been demonstrated by performing MPL on substrates pre-patterned with hydrophobic, hydrophilic or mixed SAMs. Generally, line widths are reduced by increasing the contact angle and by reducing the pen orifice dimension and inlet/substrate velocity ratio.

The advantages of MPL are that we can use any desired combination of surfactant and functional silane as ink to print selectively different functionalities at different locations. Furthermore, we can use computer-aided design (CAD) to define arbitrary 2D patterns that can be written on arbitrary surfaces. For example, we have demon-

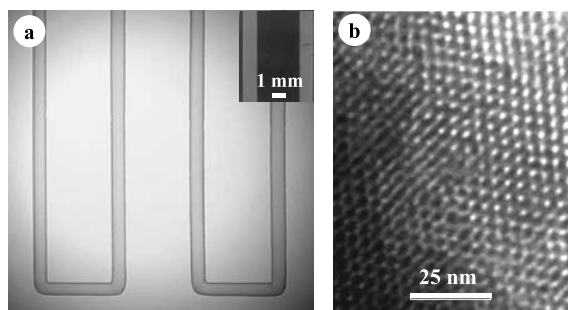


Fig. 3. Meandering patterned mesophase created by MPL. (a) Optical micrograph of patterned rhodamine-B containing silica mesophase deposited on an oxidized [100]-oriented silicon substrate at a speed of 2.54 cm s^{-1} . Inset is a fluorescence image of rhodamine-B emission acquired through a 610 nm bandpass filter, demonstrating retention of rhodamine-B functionality, and (b) representative TEM micrograph of a fragment of the patterned rhodamine-B containing film corresponding to a [110]-oriented cubic mesophase with lattice constant $a = 10.3 \text{ nm}$. The sol was prepared by adding 0.01 wt.% rhodamine-B to a silica/4 wt.% Brij-56 sol. The TEOS:EtOH:water:HCl:Brij-56:rhodamine-B molar ratio = $1:22:5.0:0.004:0.075:2.6 \times 10^{-5}$.

strated writing rhodamine-containing mesophases (refractive index $n = 1.2\text{--}1.3$) on aerogel [25] and emulsion-templated thin films ($n = 1.03\text{--}1.10$), thereby directly defining optical wave-guide structures potentially useful for lasing [26].

MPL is best suited to write continuous patterns. Patterned macroscopic arrays of discrete mesostructures can be obtained readily by combining EISA with aerosol processing schemes like IJP [8,9]. Fig. 4b shows an optical micrograph of an array of hydrophobic, mesoporous spots formed on a silicon substrate by IJP of a TFTS-modified ink. The IJP process dispenses the ink (prepared as for MPL) as monosized, spherical aerosol droplets. On striking the surface, the droplets adopt a new shape that balances surface and interfacial energies. Accompanying evaporation creates within each droplet a gradient in surfactant concentration that drives radially directed silica-surfactant self-assembly inward from the liquid-vapor interface [27]. The TEM micrograph (Fig. 4c) shows the ordered mesoporosity of a calcined, fluoroalkylated silica mesophase formed by IJP. The link to CAD, greater printing resolution achieved compared to standard ink (see Fig. 4a), and our ability to selectively functionalize the ink,

suggest applications in sensor arrays and display technologies.

MPL and IJP are serial techniques. In situations where it is desirable to create an entire pattern with the same functionality, it might be preferable to employ a parallel technique in which the deposition process occurred simultaneously in multiple locations. Fig. 5 illustrates dip coating on patterned SAMs. This rapid, parallel procedure uses microcontact printing [28] or electrochemical patterning [29] of hydroxyl- and methyl-terminated SAMs to define hydrophilic and hydrophobic patterns on the substrate surface. Then, using inks identical to those employed for MPL and IJP, preferential ethanol evaporation during dip coating enriches the depositing film in water, causing selective de-wetting of the hydrophobic regions and ensuring self-assembly of silica-surfactant mesophases exclusively on the hydrophilic patterns. In this fashion, multiple lines, arrays of dots, or other arbitrary shapes can be printed in seconds. Recent density functional theory calculations [30] have established the ultimate resolution of this differential wetting technique to be 1–2 nm.

Pattern formation on a hydrophilic/hydrophobic surface relies on the selective de-wetting of the hydrophilic coating precursor from the hydrophobic patterns. In order to demonstrate the de-wetting behavior on a stamped patterned surface, a patterned hydrophobic/hydrophilic gold substrate was immersed in a solution containing alcohol, water and propylene glycol. During dip coating, preferential alcohol evaporation enriches the depositing film in water and propylene glycol, causing spontaneous de-wetting of the hydrophobic patterns. The scheme in Fig. 6A shows the whole process of selective de-wetting of water and propylene glycol on a patterned gold surface. Fig. 6B shows an optical image of the plan view of the resulting surface after dip coating in a water/propylene glycol/ethanol solution. Although the initial solution wets both the hydrophilic and hydrophobic regions preferential evaporation of ethanol induces de-wetting of the hydrophobic regions causing the water/EG solution to reside exclusively on the hydrophilic regions. As shown, water only absorbs on hydrophilic region. In addition, de-wetting occurs not only on stripes but

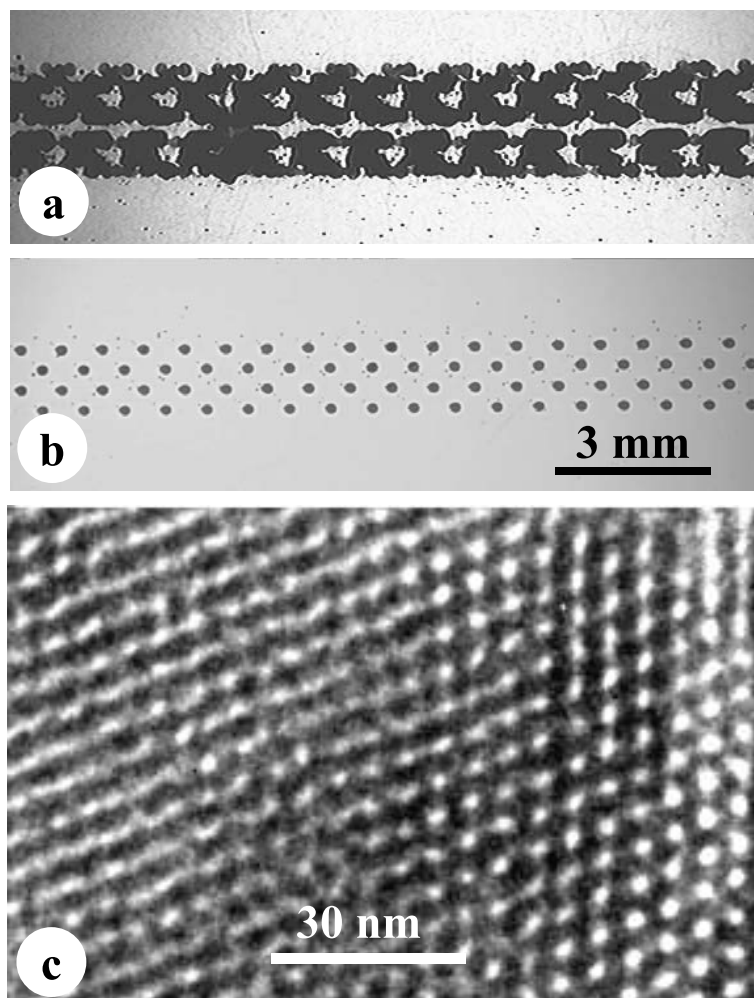


Fig. 4. Patterned dot arrays created by IJP. (a) Optical micrograph of a dot array created by IJP of standard ink (Hewlett-Packard Co.) on a non-adsorbent surface, (b) Optical micrograph of an array of hydrophobic, mesoporous silica dots created by EISA during IJP on an oxidized [1 0 0]-oriented silicon substrate followed by calcination, and (c) representative TEM micrograph of a dot fragment prepared as in (b). The sol was prepared with molar ratio TEOS:TFTS:EtOH:water:HCl:Brij-56 = 1:0.05:22.0:5.0:0.004:0.075. The dot pattern used in (a) and (b) was designed using Microsoft PowerPoint 98 software. The printing rate was approximately 80 dots s^{-1} and printer resolution 300 dots in^{-1} . The resolution achieved compared to standard ink and our ability to selectively functionalize the ink suggest applications in display technologies.

also on isolated circles. Here propylene glycol is used to suppress evaporation enabling us to image this de-wetting phenomenon.

Instead of using alcohol, water, and propylene glycol, an ink containing water, ethanol, silicate and surfactant prepared as described previously was used to prepare a patterned silica mesostructure. Fig. 7 shows the corresponding patterned features including circles and stripes of different

dimensions. The secondary ordering and length scale within the patterned macrostructure is tunable by using different sized surfactants (e.g., CTAB, Brij-56, and P123).

In addition to pure silica frameworks, the whole patterning process may be extended easily to create patterned functional organo silicate mesostructures. As an example, a fluorescent pattern was formed by adding rhodamine-B to the dip-

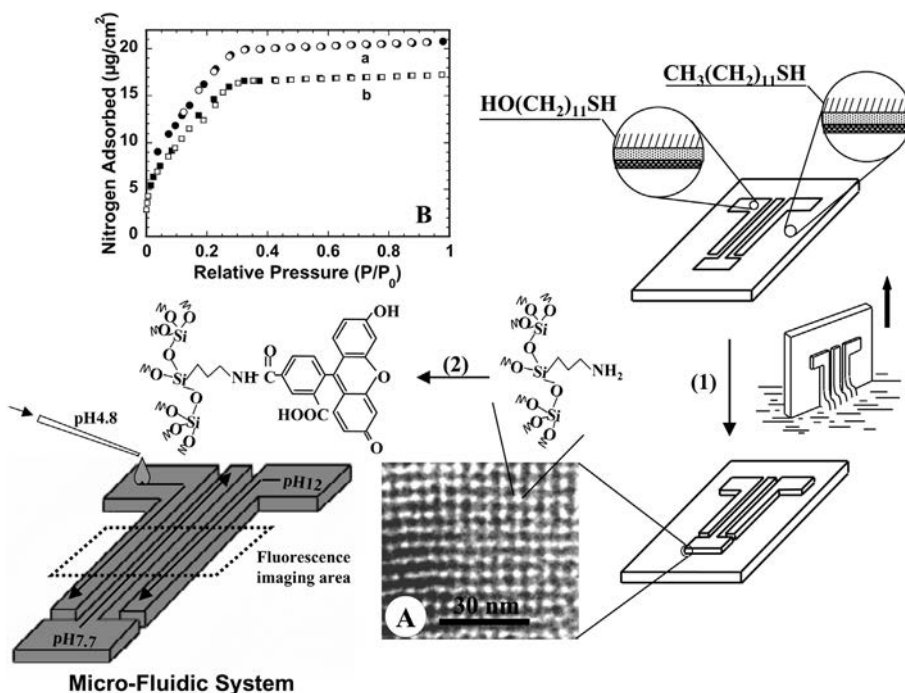


Fig. 5. Patterned functional mesostructure formed by selective de-wetting. Using microcontact printing or electrochemical desorption techniques, substrates are prepared with patterns of hydrophilic, hydroxyl-terminated SAMs and hydrophobic methyl-terminated SAMs. Preferential ethanol evaporation during dip coating (1), causes water enrichment and selective de-wetting of the hydrophobic SAMs. Correspondingly film deposition occurs exclusively on the patterned hydrophilic SAMs. The sol was prepared by adding aminopropyltrimethoxysilane ($\text{NH}_2(\text{CH}_2)_3\text{Si}(\text{OCH}_3)_3$, APS) to a silica/4 wt.% Brij-56 sol, resulting in a final molar ratio TEOS:APS:EtOH:water:HCl:Brij-56 = 1:0.8:22:5.0:0.011:0.075. Selective de-wetting followed by calcination results in a patterned, amine-functionalized, cubic mesoporous film as is evident from the plan-view TEM micrograph (inset A), showing a [100]-oriented cubic mesophase with $a = 10.3$ nm and nitrogen adsorption–desorption isotherm (inset B, curve a) acquired for the thin-film specimen using a SAW [33] technique. The dye conjugation reaction (2) was conducted by immersion in a 0.00002 mM solution of 5,6-FAM, SE (Table 1) prepared in dimethylsulfoxide (DMSO) followed by exhaustive, successive washing in DMSO, ethanol, and water. The SAW-based nitrogen adsorption–desorption isotherm of the dye-conjugated mesoporous film is shown in inset B, curve b, confirming its pore accessibility. BET analyses of the sorption isotherms indicate that the dye conjugation reaction reduces the surface area from 750 to 545 $\text{m}^2 \text{g}^{-1}$ and the hydraulic radius from 2.2 to 2.1 nm, but pore accessibility is completely retained as evident from combined TEM, SAW, and fluorescent-imaging results (Fig. 5a).

ping ink. Fig. 8 shows an optical micrograph of fluorescence emission from a patterned, mesostructured silica film containing rhodamine-B, confirming that the rhodamine-B remains optically active in the mesostructured film. The TEM image in Fig. 8 inset shows a uniform, ordered mesophase within the film.

As discussed above, Fig. 5 illustrates the formation of a patterned propyl-amine-derivatized cubic mesophase by selective de-wetting followed by calcination to remove the surfactant templates (the organosilane used was aminopropyltrimeth-

oxysilane-3 in Table 1). The TEM micrograph (Fig. 5, inset A) and N_2 -sorption isotherm (based on surface acoustic wave (SAW) measurements; Fig. 5, inset B) provide evidence of the mesostructural order and proof of the accessibility of the mesoporosity to the vapor phase. In order to make a pH-sensitive fluidic system, the covalently bound propyl-amine ligands were conjugated with a pH-sensitive dye, 5,6-carboxyfluorescein, succinimidyl ester (5,6-FAM, SE) introduced in the pore-channel network of the cubic mesophase. After removal of any non-covalently bonded dye,

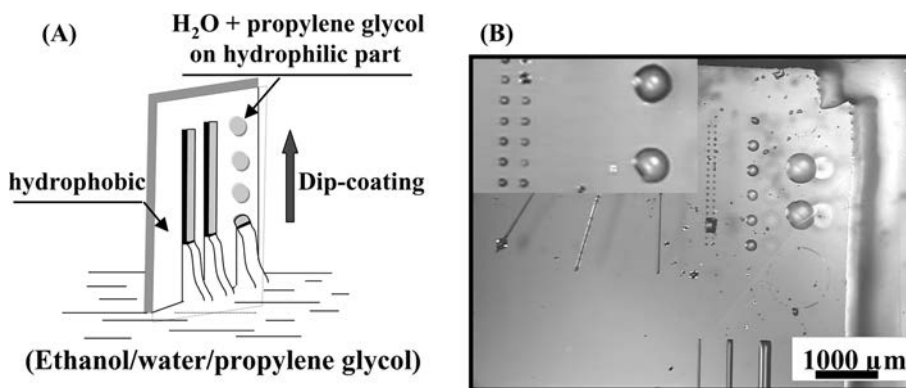


Fig. 6. (A) A dip-coating process of patterned surface in water/propylene glycol/ethanol solution, and (B) the optical image of a plan view of the resulting surface after dip coating.

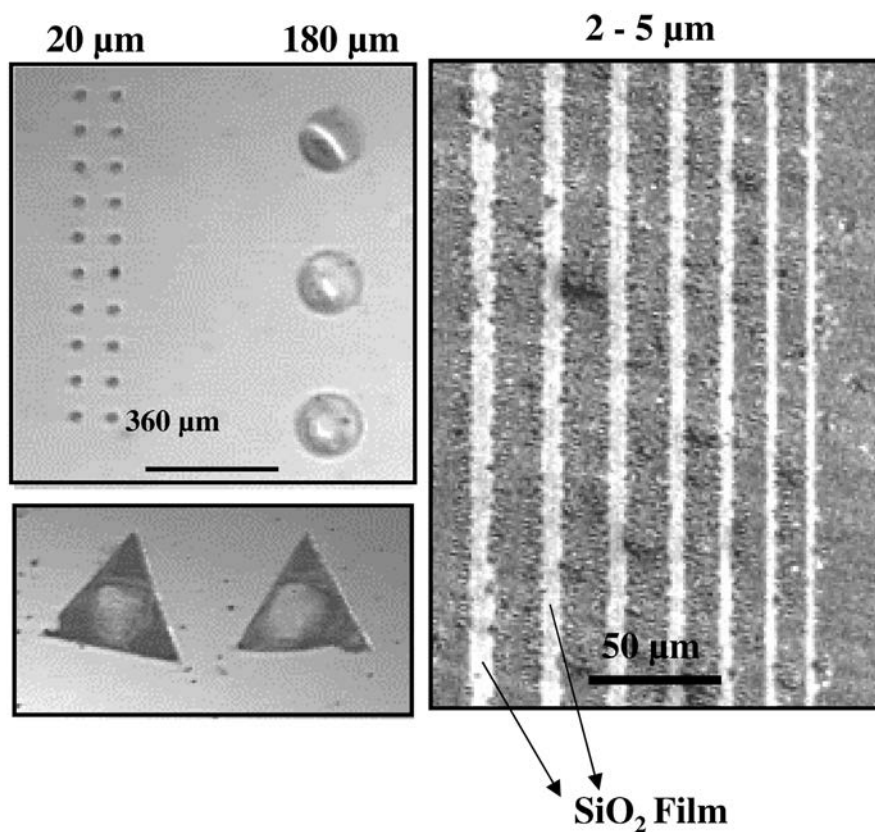


Fig. 7. SEM images of patterned mesoporous silica thin films in different features.

the uniform, continuous porosity of the amine-derivatized and dye-conjugated films was confirmed by TEM (Fig. 9c) and the corresponding

SAW-based nitrogen sorption isotherm (Fig. 5, inset B). The slight reduction in film porosity after dye conjugation reflects the volume occupied by

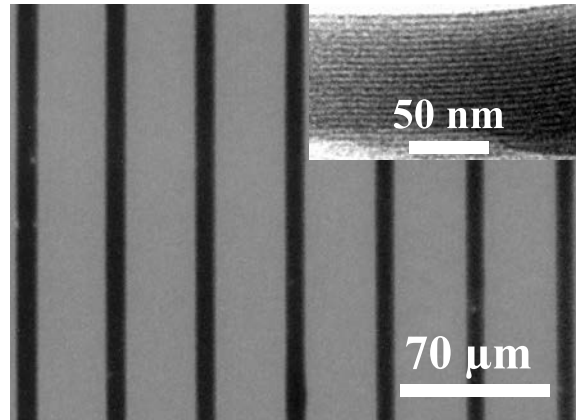


Fig. 8. Fluorescence image of patterned mesostructured silica thin films containing rhodamine-B. Inset is the TEM image of corresponding film.

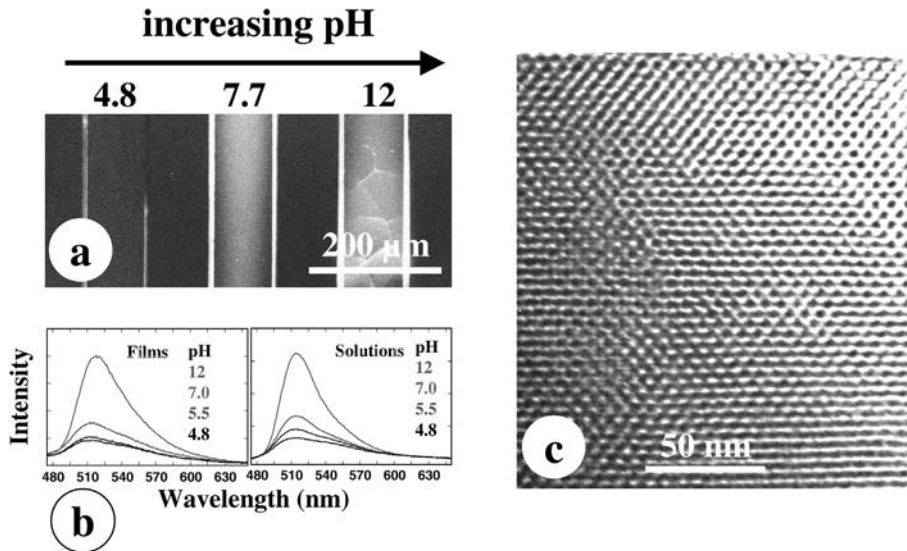


Fig. 9. Patterned pH-sensitive fluidic system. (a) Fluorescence image of three adjacent 5,6-FAM, SE-conjugated pore channel networks after introduction of aqueous solutions prepared at pH 4.8, 7.7, or 12.0. Patterned dye-conjugated thin film mesophases were prepared according to Fig. 5. Aqueous solutions of varying pH were introduced on the terminal pads (Fig. 5) and transported into the imaging cell by capillary flow. Image was acquired using a Nikon Diaphot 300 inverted microscope and 520-nm bandpass filter, (b) fluorescence spectra of 5,6-FAM, SE-conjugated mesoporous films upon exposure to aqueous solutions of pH 4.8, 7.7, and 12.0. Shown for comparison are fluorescence spectra of 0.1 μM solutions of 5,6-FAM, SE prepared in aqueous solutions of pH 4.8, 7.7, and 12.0. The similarity of the two sets of spectra confirms the maintenance of dye functionality upon conjugation within the mesoporous channel system, and (c) cross-sectional TEM micrograph of the patterned, dye-conjugated thin-film mesophase, providing evidence of the 3D pore channel network.

the attached dye moieties. The patterned, dye-conjugated array was used to monitor the pH of fluids introduced at terminal pads and transported by capillary flow into an imaging cell (Fig. 5).

Fig. 9a shows the fluorescence image of an array contacted with three different aqueous solutions prepared at pH 4.8, 7.7, and 12.0. Fig. 9b shows the corresponding emission spectra. Comparison

with solution data (Fig. 9b) indicates that dye molecules covalently attached to the mesoporous framework retain similar functionality to those in solution. The combined fluorescence image (Fig. 9a) and plan view and cross-sectional TEM micrographs (Figs. 5 and 9c) of the patterned dye-conjugated film demonstrate the uniformity of macro- and mesoscale features achievable by this evaporation-induced, de-wetting and self-assembly route. In comparison, films formed slowly (2–24 h) by nucleation and growth of thin-film mesophases on patterned SAMs [2] were observed to have non-homogeneous, globular morphologies unsuitable for fluidic or photonic systems. We also note that in this case the mesoporous film formed on the hydrophobic regions.

4. Conclusions

We have combined EISA with rapid prototyping techniques like pen lithography, IJP, and dip coating on micro-contact printed substrates to form hierarchically organized structures in seconds. By co-condensation of tetrafunctional silanes ($\text{Si}(\text{OR})_4$) with tri-functional organosilanes ($(\text{RO})_3\text{SiR}'$) or by inclusion of organic additives, we have selectively derivatized the silica framework with functional R' ligands or molecules. In addition, the formation of a new class of hybrid polysilsesquioxane film mesophases with integral organic functionality, such as mechanical properties, has been demonstrated. The patterned materials exhibit form and function on multiple length scales: on the molecular scale, functional organic moieties are positioned on pore surfaces, on the mesoscale, mono-sized pores are organized into 1D, 2D, or 3D networks, providing size-selective accessibility from the gas or liquid phase, and on the macroscale, 2D arrays and fluidic or photonic systems may be defined. We believe that the EISA process described here, and its elaboration in three different printing procedures, holds great promise for rapid prototyping of functional fluidic and photonic devices, along with displays and sensor arrays. Compared to alternative approaches like micromolding in capillaries, printing is considerably faster (seconds compared to 12 h) and avoids

the need for molds, masks, and resists. By using a spectrum of functional inks and interfacing with commercially available software, CAD and rapid transcription of functional microsystems may soon be achievable.

Acknowledgements

We thank R. Assink for performing NMR experiments, P. Yang for technical assistance with micropen lithography. We thank D. Loy for providing bridged precursors and BASF for providing Pluronic P123. TEM investigations were performed in the Department of Earth and Planetary Sciences at the University of New Mexico. This work was supported by the US Department of Energy Basic Energy Sciences Program, the Sandia National Laboratories Laboratory – Directed Research and Development Program, the Defense Advanced Research Projects Agency Bio-Weapons Defense Program, and the US Department of Defense Office of Naval Research. Sandia is a multiprogram laboratory operated by Sandia Corporation, a Lockheed–Martin Company, for the US DOE under Contract DE-AC04-94AL85000.

References

- [1] Y. Xia, G.M. Whitesides, *Angew. Chem. Int. Ed.* 37 (1998) 550.
- [2] H. Yang, N. Coombs, G.A. Ozin, *Adv. Mater.* 9 (1997) 811.
- [3] M. Trau, N. Uao, E. Lim, Y. Xia, G.M. Whitesides, I.A. Aksay, *Nature* 390 (1997) 674.
- [4] P. Yang, T. Deng, D. Zhao, P. Feng, D. Pine, B.F. Chmelka, G.M. Whitesides, G.D. Stucky, *Science* 282 (1998) 2244.
- [5] C.J. Brinker, Y. Lu, A. Sellinger, H. Fan, *Adv. Mater.* 11 (1999) 579.
- [6] R.D. Piner, J. Zhu, F. Xu, S. Hong, C.A. Mirkin, *Science* 283 (1999) 661.
- [7] P. Yang, D. Dimos, M.A. Rodriguez, R.F. Huang, S. Dai, D. Wilcox, *Mat. Res. Soc. Symp. Proc.* 542 (1999) 159.
- [8] S.-C. Chang, J. Liu, J. Bharathan, Y. Yang, J. Onohara, J. Kido, *Adv. Mater.* 11 (1999) 734.
- [9] D. Pede, G. Serra, D. De Rossi, *Mat. Sci. Eng. C5* (1998) 289.
- [10] S.L. Burkett, S.D. Sims, S. Mann, *Chem. Commun.* (1996) 1367.

- [11] C.E. Fowler, S.L. Burkett, S. Mann, *Chem. Commun.* (1997) 1769.
- [12] M.H. Lim, C.F. Blanford, A. Stein, *J. Am. Chem. Soc.* 119 (1997) 4090.
- [13] C. Kresge, M. Leonowicz, W. Roth, C. Vartuli, J. Beck, *Nature* 359 (1992) 710.
- [14] C.E. Fowler, S.L. Burkett, S. Mann, *Chem. Commun.* (1996) 1367.
- [15] J. Liu, X. Feng, G.E. Fryxell, L.-Q. Wang, A.Y. Kim, M. Gong, *Adv. Mater.* 10 (1998) 161.
- [16] B. Lebeau, C.E. Fowler, S.R. Hall, S. Mann, *J. Mater. Chem.* 9 (1999) 2279.
- [17] S. Imagaki, S. Guan, Y. Fukushima, T. Ohsuna, O. Terasaki, *J. Am. Chem. Soc.* 121 (1999) 9611.
- [18] B.J. Melde, B.T. Holland, C.F. Blanford, A. Stein, *Chem. Mater.* 11 (1999) 3302.
- [19] T. Asefa, M.J. MacLachlan, N. Coombs, G.A. Ozin, *Nature* 402 (1999) 867.
- [20] Y. Lu, R. Ganguli, C.A. Drewien, M.T. Anderson, C.J. Brinker, W.L. Gong, Y.X. Guo, H. Soyez, B. Dunn, M.H. Huang, J.I. Zink, *Nature* 389 (1997) 364.
- [21] P.T. Tanev, T.J. Pinnavaia, *Science* 267 (1995) 865.
- [22] C.D. Bain, E.B. Troughton, Y.-T. Tao, J. Ewall, G.M. Whitesides, R.G. Nuzzo, *J. Am. Chem. Soc.* 111 (1989) 321.
- [23] H. Yang, N. Coombs, I. Sokolov, G.A. Ozin, *Nature* 381 (1996) 589.
- [24] A. Sellinger, P.N. Weiss, A. Nguyen, Y. Lu, R.A. Assink, W. Gong, C.J. Brinker, *Nature* 394 (1998) 256.
- [25] S.S. Prakash, C.J. Brinker, A.J. Hurd, S.M. Rao, *Nature* 374 (1995) 439.
- [26] P. Yang, G. Wirnsberger, H.C. Huang, S.R. Cordero, M.D. McGehee, B. Scott, T. Deng, G.M. Whitesides, B.F. Chmelka, S.K. Buratto, G.D. Stucky, *Science* 287 (2000) 465.
- [27] Y. Lu, H. Fan, A. Stump, T.L. Ward, T. Reiker, C.J. Brinker, *Nature* 398 (1999) 223.
- [28] J.L. Wilbur, A. Kumar, H.A. Biebuyck, E. Kim, G.M. Whitesides, *Nanotechnology* 7 (1996) 452.
- [29] L.M. Tender, R.L. Worley, H. Fan, G.P. Lopez, *Langmuir* 12 (1996) 5515.
- [30] L.J. Douglas Frink, A.G. Sallinger, *J. Chem. Phys.* 110 (1999) 5969.
- [31] R.A. Cairncross, P.R. Schunk, T.A. Baer, R.R. Rao, P.A. Sackinger, *Int. J. Numer. Meth. Fluids* 33 (2000) 375.
- [32] T.A. Baer, R.A. Cairncross, P.R. Schunk, R.R. Rao, P.A. Sackinger, *Int. J. Numer. Meth. Fluids* 33 (2000) 405.
- [33] G.C. Frye, A.J. Ricco, S.J. Martin, C.J. Brinker, in: C.J. Brinker, D.E. Clark, D.R. Ulrich (Eds.), *Better Ceramics Through Chemistry III*, Vol. 121, Mat. Res. Soc. Reno, Nevada, 1988, p. 349.